Multiple-charge modulations in the ferromagnetic insulating state of lightly doped $La_{1-x}Sr_xMnO_3$

T. Asaka,[1,2,3] S. Mori,[4] Y. Horibe,[5] K. Takenaka,[6] X. Z. Yu,[2] T. Nagai,[7] K. Kimoto,[2,7] T. Hirayama,[1] and Y. Matsui[2]

[1]*Nanostructures Research Laboratory, Japan Fine Ceramics Center (JFCC), Nagoya 456-8587, Japan*

[2]*Advanced Nano Characterization Center, National Institute for Materials Science (NIMS), Tsukuba 305-0044, Japan*

[3]*Department of Materials Science and Engineering, Nagoya Institute of Technology, Nagoya 466-8555, Japan*

[4]*Department of Materials Science, Osaka Prefecture University, Osaka 599-8531, Japan*

[5]*Rutgers Center for Emergent Materials and Department of Physics and Astronomy, Rutgers University, Piscataway, New Jersey 08854, USA*

[6]*Department of Crystalline Materials Science, Nagoya University, Nagoya 464-8603, Japan*

[7]*Transmission Electron Microscopy Cluster, National Institute for Materials Science (NIMS), Tsukuba 305-0047, Japan*

(Received 18 June 2010; revised manuscript received 22 March 2011; published 2 May 2011)

We investigated the texture of charge modulations and behaviors of their domains in the ferromagnetic insulating state of $La_{1-x}Sr_xMnO_3$ ($x = 0.125$) by low-temperature transmission electron microscopy. We observed simultaneous evolutions of three charge-modulated phases below ~135 K, close to the charge-ordering-transition temperature $T_{CO} \sim 140$ K. The phases form intricate domain structures within one ferromagnetic phase. This indicates that one magnetic state exhibits multiple-charge states. With further decreasing temperature, below ~40 K, the three charge-modulated phases behave differently from one another. We consider that the behaviors would lead to a phase separation into the ferromagnetic insulating phase and the ferromagnetic metallic one.

DOI: 10.1103/PhysRevB.83.174401 PACS number(s): 71.30.+h, 61.05.jm, 75.50.Dd, 75.60.Ch

I. INTRODUCTION

Self-organizations of charge, orbital, and spin are often observed in correlated electron materials. They can trigger exotic electric and magnetic properties, such as the charge stripes in high-temperature superconductors,[1] and the charge/orbital modulations and charge segregations in manganites.[2–4] Typically, the charge and spin states are mutually coupled in the correlated electron system. Therefore, the charge states are likely to define the spin states and vice versa. For example, the charge order often observed in manganites is accompanied by the antiferromagnetic spin order,[5,6] and the ferromagnetic state shows a metallic nature resulting from electron itinerancy, which is interpreted in terms of the double-exchange (DE) interaction.[7]

The lightly doped $La_{1-x}Sr_xMnO_3$ exhibits the ferromagnetic insulating (FMI) state at low temperatures. This ferromagnetism is inconvertible with the insulating property within the framework of the conventional DE interaction. Upon cooling, $La_{1-x}Sr_xMnO_3$ with the doping level $x = 0.11$–0.15 exhibits the transition from the ferromagnetic metallic (FMM) phase to the FMI phase at the charge-ordering-transition temperature T_{CO} (e.g., $T_{CO} \sim 140$ K for $x = 0.125$).[8–12] Interestingly, in the lightly doped $La_{1-x}Sr_xMnO_3$, the FMI phase is more stable in a magnetic field than the FMM phase. Hence, the positive magnetoresistance (MR) has been observed at around T_{CO}.[13,14] The insulating nature of the FMI state has been considered to be due to the existence of charge and/or orbital orders.[15–26] In fact, the structural modulations caused by the charge/orbital orders have been observed. First, a neutron diffraction study[15] has demonstrated superlattice reflections with a modulation wave vector (0,0,1/2) in the FMI phase. Furthermore, an electron-diffraction study[16] for the FMI state has shown a superstructure with $\sim 2a_c \times 4b_c \times 4c_c$ in a simple perovskite unit cell notation. For this superstructure, more recently, Geck *et al.*[18] have proposed a structure model of the three-dimensional (3-D) charge/orbital ordering, in which the DE interaction is allowed locally. Since the first finding of the structural modulation, a number of experimental and theoretical studies about the charge/orbital orders in the lightly doped $La_{1-x}Sr_xMnO_3$ have been reported.[12,16–26] However, we have not yet reached a consensus about the origin and structure of the charge/orbital orders in this system.

In this paper, we report a novel charge state, which is a multiple-charge-modulated state, observed in the FMI state of the lightly doped $La_{1-x}Sr_xMnO_3$ ($x = 0.125$). We examined the spatial developments and temperature evolutions of the ferromagnetic charge (orbital)-ordered phase. We found that the charge (orbital)-ordered phase can be divided into three charge (orbital) orders, i.e., multiple-charge (orbital) ordering. These charge orders are commonly accompanied by a long-range ferromagnetic order. Such a multiple-charge (orbital)-ordered state within one magnetic phase has never been reported as far as we know. Hereinafter, we simply express the charge (orbital) order in the FMI state by "the charge modulation" to facilitate understanding.

II. EXPERIMENTS

We employed low-temperature transmission electron microscopy (TEM) involving selected area electron diffraction (SAED) and Lorentz microscopy for the observation of the FMI phase in $La_{0.875}Sr_{0.125}MnO_3$. TEM allows us to concurrently obtain crystallographic and magnetic information in both the reciprocal and real spaces.[27] The examined crystal was grown by a floating-zone method and exhibited the transition from the FMM phase to the FMI phase at $T_{CO} \sim 140$ K.[28]

For the observation and measurement using TEM, the crystalline sample was thinned by mechanical grinding and Ar^+ ion sputtering. The specimen thickness in the observed area was ~150 nm or less. The specimens were cooled from room temperature to 18 K in liquid-nitrogen- or liquid-helium-cooling holders and examined using a field-emission gun

Lorentz electron microscope (Hitachi HF-3000L) operating at 300 kV. The microscope is equipped with a custom-made objective lens, which makes magnetic fields at the sample position almost 0. Lorentz-Foucault and Lorentz-Fresnel methods were used for the observation of the magnetic domains. All data were recorded on imaging plates.

III. RESULTS AND DISCUSSION

First, we confirmed the crystal structure in the FMI state by SAED. Figures 1(a)–1(c) show the typical electron-diffraction patterns of the FMI phase, obtained at 80 K. We observed sharp weak superlattice reflections, as indicated by arrowheads, in addition to strong fundamental reflections. The superlattice reflections in the electron-diffraction patterns reveal three modulation wave vectors, namely, $\boldsymbol{q}_1 = (0,0,1/2)_o = (0,0,1/4)_c$, $\boldsymbol{q}_2 = (1/2,-1/2,0)_o = (1/2,0,0)_c$ [$\boldsymbol{q}'_2 = (1/2,1/2,0)_o = (0,1/2,0)_c$], and $\boldsymbol{q}_3 = (1/4,1/4,0)_o = (0,1/4,0)_c$, as summarized in Ref. 18. Here, the subscripts "o" and "c" represent the notations of the orthorhombic and pseudocubic perovskite unit cells, respectively. Figure 1(d) shows a schematic diagram of the reciprocal lattice of the FMI phase. The large and small circles represent the fundamental and superlattice reflections, respectively. The superlattice reflections are explained with a supercell of $2a_c \times 4b_c \times 4c_c$, as demonstrated in Ref. 16. Note that the superlattice reflections originate from periodic structural distortions, i.e., structural modulations, in the electron diffraction. With increasing temperature, these superlattice reflections disappeared at

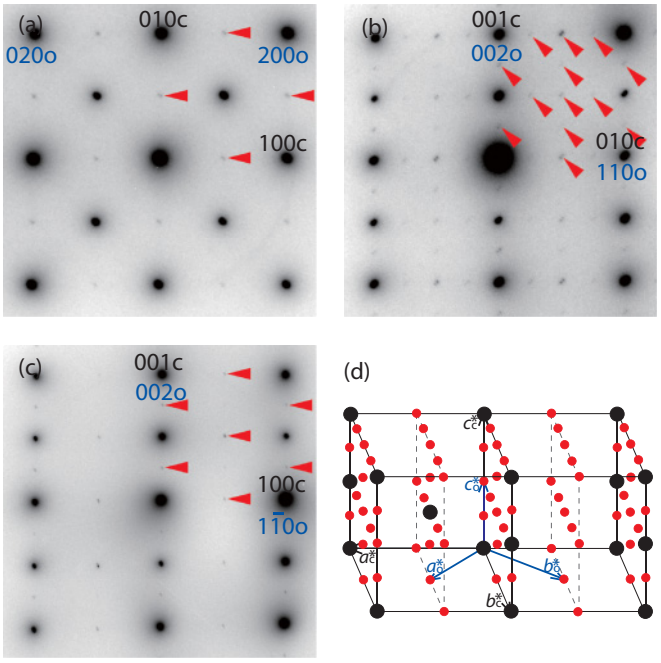

FIG. 1. (Color online) Typical electron-diffraction patterns of the ferromagnetic insulating phase in $La_{0.875}Sr_{0.125}MnO_3$. (a) $[001]_o$-($[001]_c$-), (b) $[\bar{1}10]_o$- ($[100]_c$-), and (c) $[110]_o$- ($[010]_c$-) zones electron-diffraction patterns obtained at 80 K. Arrowheads indicate superlattice reflection spots. (d) Schematic illustration of entire reciprocal lattice. Large black and small red circles denote fundamental and superlattice spots, respectively. See the text about the reflection indexes and the crystal axes.

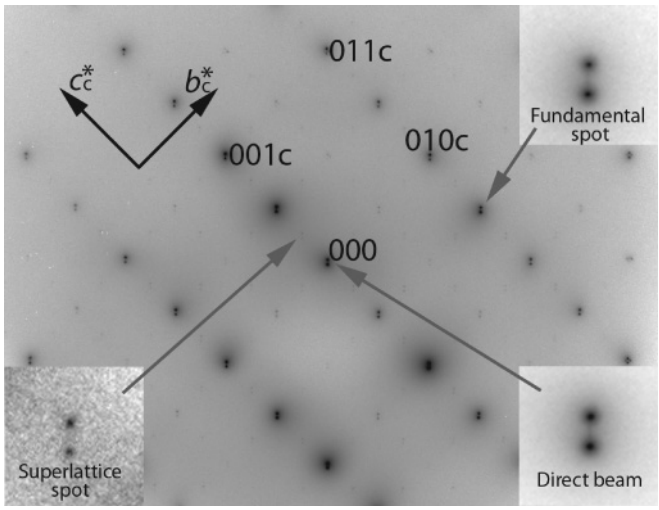

FIG. 2. (Color online) $[100]_c$-zone high-resolution electron-diffraction pattern at 80 K. Insets show the magnified images of the direct beam and the fundamental and superlattice reflection spots. The contrast of each image was independently adjusted to facilitate visualization.

~135 K, close to T_{CO} (~140 K). Thus, the structural modulations are characteristic of the FMI phase and would be accompanied by the charge modulations.

To confirm that the charge-modulated phase exhibits ferromagnetism, we performed high-resolution electron diffraction for the FMI state. Figure 2 shows a magnified $[100]_c$-zone SAED pattern across two ferromagnetic (FM) domains at 80 K. Splits in the superlattice reflections, as well as the direct beam and the fundamental Bragg reflections, are clearly visible. These splits are a result of deflection of the electron beam by the Lorentz force, which is caused by magnetization in the domains. Therefore, the magnetic domains have the magnetization perpendicular to the direction of the deflection of the electron beam. The split of superlattice reflections signifies that the charge-modulated phase has a spontaneous magnetization.

To clarify the spatial distribution of the charge-modulated and FM domains, we carried out the dark-field (DF) imaging and the Lorentz-Foucault imaging. Figure 3(a) shows a Lorentz-Foucault image displaying FM domains, obtained by using one direct beam (upper beam in Fig. 2). In the Lorentz-Foucault image, both dark and bright regions indicate the FM domains with magnetization directions as denoted by arrows. We note that each FM domain in this Lorentz-Foucault image seems to be homogeneous. This image undoubtedly reveals that a long-range ferromagnetism develops in the FMI state. Figure 3(b) shows a $[100]_c$-zone DF image formed with the superlattice reflection spot of $01\frac{1}{4}{}_c$ at 80 K. This image was obtained from the boxed region in Fig. 3(a). We also display in Fig. 3(c) the median-filtered image of the DF image to easily distinguish a domain structure. Bright parts are domains with the charge modulation. Dark lines and regions show the antiphase boundaries and other phases. [As a typical example of the contrast variation in the DF image, an image-intensity profile was shown in Fig. 3(f).] Such domain images exhibit an inhomogeneous interior and blurring around the edges. The size of the domains typically ranges from tens of nanometers

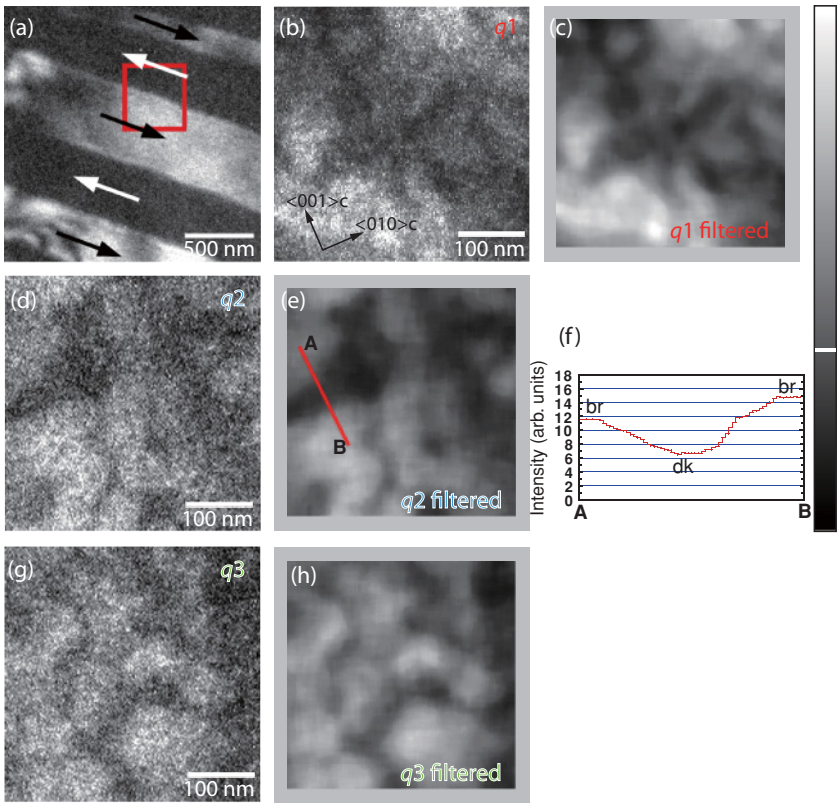

FIG. 3. (Color online) Ferromagnetic and charge-ordering domain images in the ferromagnetic insulating phase. (a) $[100]_c$-zone Lorentz-Foucault image obtained at 80 K. The image was obtained with the split upper direct beam in Fig. 2. Arrows indicate the direction of magnetization in each domain. (b)–(e), (g), and (h) Superlattice dark-field images at 80 K, obtained from the boxed region in (a). The dark-field images of (b), (d), and (g) were formed with the superlattice reflection spots $01\frac{1}{4}1_c$ ($\boldsymbol{q}_1$), $0\frac{1}{2}1_c$ ($\boldsymbol{q}_2'$), and $0\frac{1}{4}1_c$ ($\boldsymbol{q}_3$), respectively. The images of (c), (e), and (h) are the median filtered images of (b), (d), and (g), respectively, in which noises in the original images were reduced. They are displayed to easily distinguish the domains. (f) An intensity profile on the red line between A and B in (e). "br" and "dk" denote bright and dark in the contrast level, respectively. The right-hand bar is the scale of the image contrast for the dark-field images. The white line indicates the contrast level used for a criterion for describing the image contrast as "bright" or "dark". Bright parts are domains with the superstructure originating from the charge modulations.

to several hundreds of nanometers. In the same way, Figs. 3(d) and 3(g) show the $[100]_c$-zone DF images of the same region as above, formed with the superlattice spots of $0\frac{1}{2}1_c$ and $0\frac{1}{4}1_c$, respectively. Figures 3(e) and 3(h) are the filtered image of Figs. 3(d) and 3(g), respectively. Here, the superlattice spots $01\frac{1}{4}_c$, $0\frac{1}{2}1_c$, and $0\frac{1}{4}1_c$ are the representatives of the modulation-wave vectors $\boldsymbol{q}_1$, $\boldsymbol{q}_2$, and $\boldsymbol{q}_3$, respectively. By observing the DF and Lorentz-Foucault images comprehensively, we realize that all the charge-modulated domains coincide with the homogeneous FM domains. Such observations prove that the FM interaction develops widely across the charge-modulated domains.

Concerning the charge modulation structure, if three modulation wave vectors, $\boldsymbol{q}_1$, $\boldsymbol{q}_2$, and $\boldsymbol{q}_3$ are attributable to one modulated-structure phase, the respective images of the domains should be almost identical. In practice, the present images, by contrast, are distinct from one another. The charge-modulated domains observed in Figs. 3(b), 3(d), and 3(g) seem to partly overlap one another and mutually form intricate structures. In addition, each modulated phase has a different fraction in the cross-sectional area. As a rough estimate, the fractions of the q_1-, q_2-, and q_3-modulated domain contrasts for the present area are 80, 59, and 68%, respectively. For these reasons, we consider that these three modulation wave vectors do not originate from one structural phase. Thus, the triple-charge-modulated domain state is realized in the FMI state of this sample. Here, we should note that the modulation wave vectors previously reported have been discussed to exist in one structural phase thus far.[12,15–26]

Each modulation wave vector exhibits a different temperature dependence. We measured the temperature profiles of the electron diffraction at low temperatures. Figure 4(c) shows the intensity profiles of electron diffraction on the dotted lines in Fig. 4(a), i.e., along $00l_c$ and $0k2_c$, at various temperatures. With decreasing temperature below 70 K, the intensities of the q_2- and q_3-superlattice spots gradually decrease, while that of the q_1-superlattice spots apparently increases. At 19 K, the q_2'-superlattice spots become extremely weak, and the q_3-superlattice spots vanish. In addition to the intensity profiles, we show the temperature dependence of the full widths at half maximum (FWHMs) of the fundamental and superlattice spots in Fig. 4(d). At temperatures between 40 and 70 K, the observed diffraction, which includes the fundamental and superlattice reflections, forms sharp spots, indicating long-range ordering. Below 40 K, the FWHMs of the q_2'- and q_3-superlattice spots rapidly increase, that is, these spots shift toward diffuse scattering, while those of the fundamental and q_1-superlattice spots almost remain constant. This suggests that the short-range ordering of the q_2- and q_3-superlattice modulations evolves below a critical temperature ($T_{crt} \sim$ 40 K). Here, the behaviors of these superlattice modulations in the heating process are similar to those in the cooling process. That is, the behavior of the q_1-superlattice modulation is different from those of the q_2 and q_3 modulations.

To examine the change in magnetism at T_{crt}, we measured the temperature dependence of the magnetic domain structure by Lorentz-Fresnel imaging. Figure 5 shows Lorentz-Fresnel images at 18 K and 55 K. Both the bright and dark lines in the Lorentz-Fresnel images correspond to the magnetic domain walls. The magnetic domain structure is obviously different between the two images. The magnetic domains at 18 K are narrower than those at 55 K. Moreover, the directions of domain development are locally different between the two images. This suggests the change in the easy direction

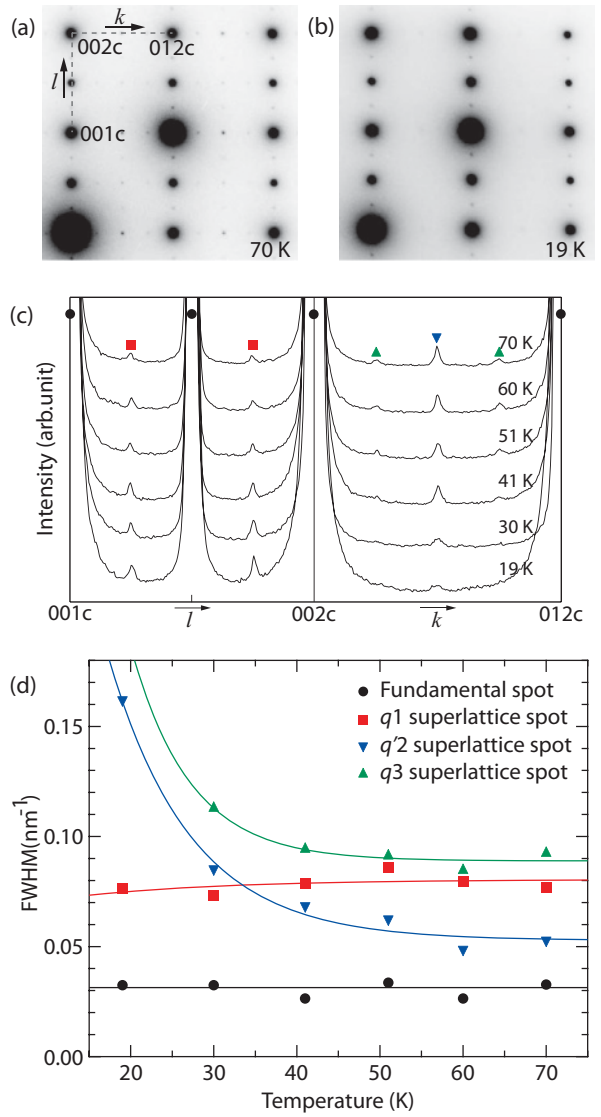

FIG. 4. (Color online) Temperature dependence of modulation structures. $[100]_c$-zone electron-diffraction patterns obtained at (a) 70 K and (b) 19 K. (c) Intensity profiles of diffraction spots along $00l_c$ and $0k2_c$ at various temperatures. Circles, squares, triangles, and inverted triangles indicate the fundamental and q_1-, q_2'-, and q_3-superlattice reflections, respectively. (d) Temperature dependence of the full widths at half maximum of the fundamental and q_1-, q_2'-, and q_3-superlattice reflections. Lines are guides for the eye.

of magnetization. The change in magnetic domain structure was observed at ~30 K. The magnetic domain structure is a natural consequence of the various contributions to the total free energy, such as magnetostatic, exchange, anisotropic, and magnetoelastic interactions.[29,30] We consider that the variation is likely caused by the change in magnetic anisotropic or magnetoelastic interactions, because of the change in the easy direction of magnetization between temperatures below and above ~30 K. In addition, we note that all the observation areas show the magnetic domains at 18 K, suggesting that the magnetic state below T_{crt} is not a phase separation, but a homogeneous ferromagnetic phase.

Finally, we discuss the development of the charge modulations at low temperatures. The observed phase behavior is summarized as follows. With decreasing temperature, when the transition from the FMM phase to the FMI phase occurs at ~135 K, the q_1-, q_2-, and q_3-charge modulations with the long-range ordering emerge concurrently so as to accord with the ferromagnetic spin interaction. Moreover, they develop independently and overlap each other in most of the regions, forming the intricate domain structures illustrated in Fig. 6(f). Here, the respective charge modulations are accompanied by structural modulations, as shown in Figs. 6(a), 6(b), and 6(c), derived from the modulation wave vectors $\boldsymbol{q}_1 = (0,0,1/4)_c$, $\boldsymbol{q}_2 = (1/2,0,0)_c$ $[\boldsymbol{q}_2' = (0,1/2,0)_c]$, and $\boldsymbol{q}_3 = (0,1/4,0)_c$, respectively. With further cooling, below ~40 K, the q_2- and q_3-charge modulations gradually diminish [Fig. 6(e)] and subsequently vanish. Consequently, only the q_1-modulation domains persist, as shown in Fig. 6(d). The observed triple-charge-modulated state, i.e., the coexistence of the three phases, might be due to a chemical disorder[31] or strain fields,[32] like the phase coexistences of the FMM phase and the antiferromagnetic charge-ordering insulating phase, which are often observed in the manganites.[3,33] In particular, if the intrinsic strain fields, which are caused by the lattice effect or the Jahn-Teller distortion in many cases,[32,34–38] are the origin of the phase coexistence, it may be related to the pseudocubic crystal structure in the FMI phase where the pseudocubic crystal axes are very close ($a = 5.534$, $b = 5.518$, and $c/\sqrt{2} = 5.507$ Å for the triclinic phase at 75 K in $x = 0.125$).[12] Such a crystal structure would give rise to the degeneracy of the modes of the charge modulations. Moreover, the induced strain fields caused by the form effect, such as the thin film effect, can also result in the texture of the multiple-phase state.[39–42] In such a case, the different lattice modulations may couple differently to possible strain fields. This might explain the observed intricate domain structures. Besides, the state observed below 40 K can be regarded as a phase separation between the q_1-modulation phase and the

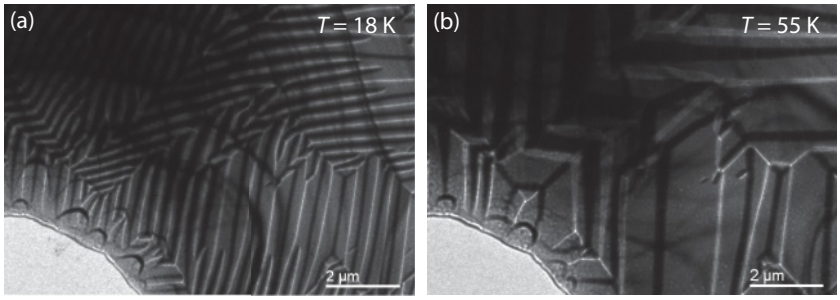

FIG. 5. (Color online) Lorentz-Fresnel images obtained at (a) 18 K ($<T_{crt} \sim 40$ K) and (b) 55 K ($>T_{crt}$). Both bright and dark lines correspond to the magnetic domain walls.

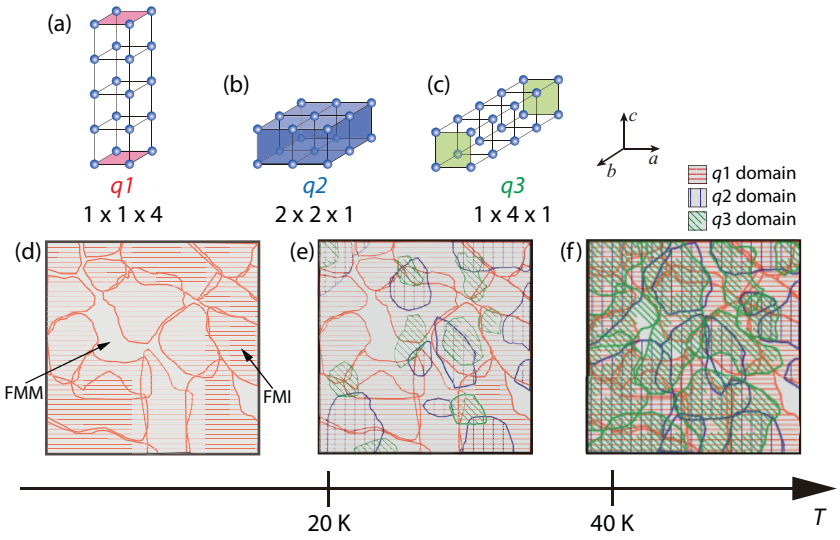

FIG. 6. (Color online) (a)–(c) Schematic illustrations of supercells corresponding to respective charge modulations. The (a) q_1, (b) q_2, and (c) q_3 supercells are represented using the pseudocubic structure. Circles denote manganese ions. The c axis of the q_1 supercell is fourfold that of the pseudocubic unit cell. The q_2 supercell has twofold a and b axes. The q_3 supercell has a fourfold b axis. These supercells are accompanied by the corresponding charge modulations. (d)–(f) Schematic illustrations of possible models of charge modulation developments around and below 40 K. Striped regions represent the domains of the respective charge modulations. Here, the illustration of (f) was roughly traced from Figs. 3(b), 3(d), and 3(g).

no-charge-modulation one which results from the decay of the q_2- and q_3-charge modulations. We speculate that the no-charge-modulation phase is an alternative FMM state with itinerant electrons, as shown in Fig. 6(d). In fact, a recent NMR study[43] has demonstrated the phase separation into the FMI and FMM phases below ∼30 K. Here, we should note the possibility that an electron-irradiation effect may cause the observed phase separation, as shown in the x-ray studies,[25,44,45] because, at low-temperatures, the charge modulations might be significantly sensitive to the electron irradiation.[46,47] In any case, the three charge modulations differ from one another in the distributions and the temperature dependence.

IV. SUMMARY

In this study, we observed three charge modulations in the ferromagnetic insulating state of $La_{1-x}Sr_xMnO_3$ ($x = 0.125$), which have three different behaviors with respect to spatial development and temperature evolution. The charge modulations form intricate domain structures within the ferromagnetic phase that exhibits an ordinary long-range magnetic interaction. Thus, we observed a triple-charge-modulated state with the ferromagnetic spin interaction. Moreover, we observed the phase separation into two distinct ferromagnetic phases, with and without the charge modulations, below ∼40 K. Although the origin of the phase separation is still unclear, this results from the decay of two of the three charge modulations.

ACKNOWLEDGMENTS

We thank K. Tsuda, T. Arima, Y. Zhu, and C. A. J. Fisher for their valuable discussions, and C. Tsuruta and W. Zhang for their collaboration. A part of this work was supported by the Nanotechnology Support Project; of the Ministry of Education, Culture, Sports, Science, and Technology (MEXT) of Japan.

[1] J. M. Tranquada, B. J. Sternlieb, J. D. Axe, Y. Nakamura, and S. Uchida, Nature (London) **375**, 561 (1995).
[2] Y. Tokura and N. Nagaosa, Science **288**, 462 (2000).
[3] M. Uehara, S. Mori, C. H. Chen, and S.-W. Cheong, Nature (London) **399**, 560 (1999).
[4] E. Dagotto, *Nanoscale Phase Separation and Colossal Magnetoresistance* (Springer-Verlag, Berlin, 2003).
[5] E. O. Wollan and W. C. Koehler, Phys. Rev. **100**, 545 (1955).
[6] J. B. Goodenough, Phys. Rev. **100**, 564 (1955).
[7] C. Zener, Phys. Rev. **82**, 403 (1951).
[8] A. Urushibara, Y. Moritomo, T. Arima, A. Asamitsu, G. Kido, and Y. Tokura, Phys. Rev. B **51**, 14103 (1995).
[9] B. Dabrowski, X. Xiong, Z. Bukowski, R. Dybzinski, P. W. Klamut, J. E. Siewenie, O. Chmaissem, J. Shaffer, C. W. Kimball, J. D. Jorgensen, and S. Short, Phys. Rev. B **60**, 7006 (1999).
[10] G.-L. Liu, J.-S. Zhou, and J. B. Goodenough, Phys. Rev. B **64**, 144414 (2001).
[11] M. Paraskevopoulous, F. Mayr, J. Hemberger, A. Loidl, R. Heichele, D. Maurer, V. Müller, A. A. Mukhin, and A. M. Balbashov, J. Phys. Condens. Matter **12**, 3993 (2000).
[12] D. E. Cox, T. Iglesias, E. Moshopoulou, K. Hirota, K. Takahashi, and Y. Endoh, Phys. Rev. B **64**, 024431 (2001).
[13] S. Uhlenbruck, R. Teipen, R. Klingeler, B. Büchner, O. Friedt, M. Hücker, H. Kierspel, T. Niemöller, L. Pinsard, A. Revcolevschi, and R. Gross, Phys. Rev. Lett. **82**, 185 (1999).
[14] H. Nojiri, K. Kaneko, M. Motokawa, K. Hirota, Y. Endoh, and K. Takahashi, Phys. Rev. B **60**, 4142 (1999).
[15] Y. Yamada, O. Hino, S. Nohdo, R. Kanao, T. Inami, and S. Katano, Phys. Rev. Lett. **77**, 904 (1996).
[16] K. Tsuda, M. Tanaka, K. Hirota, and Y. Endoh, J. Phys. Soc. Jpn. **70**, 1010 (2001).
[17] T. Mizokawa, D. I. Khomskii, and G. A. Sawatzky, Phys. Rev. B **61**, R3776 (2000).
[18] J. Geck, P. Wochner, S. Kiele, R. Klingeler, P. Reutler, A. Revcolevschi, and B. Büchner, Phys. Rev. Lett. **95**, 236401 (2005).

[19]T. Inami, N. Ikeda, Y. Murakami, I. Koyama, Y. Wakabayashi, and Y. Yamada, Jpn. J. Appl. Phys. Suppl. **38-1**, 212 (1999).
[20]Y. Yamada, J. Suzuki, K. Oikawa, S. Katano, and J. A. Fernandez-Baca, Phys. Rev. B **62**, 11600 (2000).
[21]Y. Endoh, K. Hirota, S. Ishihara, S. Okamoto, Y. Murakami, A. Nishizawa, T. Fukuda, H. Kimura, H. Nojiri, K. Kaneko, and S. Maekawa, Phys. Rev. Lett. **82**, 4328 (1999).
[22]M. Korotin, T. Fujiwara, and V. Anisimov, Phys. Rev. B **62**, 5696 (2000).
[23]T. Niemöller, M. von Zimmermann, S. Uhlenbruck, O. Friedt, B. Büchner, T. Frello, N. H. Andersen, P. Berthet, L. Pinsard, A. M. De Léon-Guevara, A. Revcolevschi, and J. R. Shneider, Eur. Phys. J. B **8**, 5 (1999).
[24]F. Moussa, M. Hennion, F. Wang, P. Kober, J. Rodríguez-Carvajal, P. Reutler, L. Pinsard, and A. Revcolevschi, Phys. Rev. B **67**, 214430 (2003).
[25]J. Geck, P. Wochner, D. Bruns, B. Büchner, U. Gebhardt, S. Kiele, P. Reutler, and A. Revcolevschi, Phys. Rev. B **69**, 104413 (2004).
[26]S. Grenier, K. J. Thomas, J. P. Hill, U. Staub, Y. Bodenthin, M. García-Fernández, V. Scagnoli, V. Kiryukhin, S.-W. Cheong, B. G. Kim, and J. M. Tonnerre, Phys. Rev. Lett. **99**, 206403 (2007).
[27]T. Asaka, X. Z. Yu, Y. Tomioka, Y. Kaneko, T. Nagai, K. Kimoto, K. Ishizuka, Y. Tokura, and Y. Matsui, Phys. Rev. B **75**, 184440 (2007).
[28]R. Shiozaki, K. Takenaka, Y. Sawaki, and S. Sugai, Phys. Rev. B **63**, 184419 (2001).
[29]A. Hubert and R. Schafer, *Magnetic Domains: The Analysis of Magnetic Microstructures* (Springer-Verlag, Berlin, 1998).
[30]S. Chikazumi, *Physics of Ferromagnetism* (Oxford University Press, New York, 1997).
[31]A. Moreo, S. Yunoki, and E. Dagotto, Science **283**, 2034 (1999).
[32]K. H. Ahn, T. Lookman, and A. R. Bishop, Nature (London) **428**, 401 (2004).
[33]S. Mori, T. Asaka, and Y. Matsui, J. Electron Microsc. **51**, 225 (2002).
[34]J. Burgy, A. Moreo, and E. Dagotto, Phys. Rev. Lett. **92**, 097202 (2004).
[35]J. Tao and J. M. Zuo, Phys. Rev. B **69**, 180404(R) (2004).
[36]M. Pissas, I. Margiolaki, K. Prassides, and E. Suard, Phys. Rev. B **72**, 064426 (2005).
[37]W. J. Lu, Y. P. Sun, B. C. Zhao, X. B. Zhu, and W. H. Song, Phys. Rev. B **73**, 214409 (2006).
[38]T. Nagai, T. Kimura, T. Asaka, K. Kimoto, M. Takeguchi, and Y. Matsui, Phys. Rev. B **81**, 060407(R) (2010).
[39]P. R. Sagdeo, S. Anwar, and N. P. Lalla, Phys. Rev. B **74**, 214118 (2006).
[40]T. Zhang and M. Dressel, Phys. Rev. B **80**, 014435 (2009).
[41]A. Biswas, M. Rajeswari, R. C. Srivastava, Y. H. Li, T. Venkatesan, R. L. Greene, and A. J. Millis, Phys. Rev. B **61**, 9665 (2000).
[42]H. Jeen and A. Biswas, Phys. Rev. B **83**, 064408 (2011).
[43]G. Papavassiliou, M. Pissas, G. Diamantopoulos, M. Belesi, M. Fardis, D. Stamopoulos, A. G. Kontos, M. Hennion, J. Dolinsek, J.-Ph. Ansermet, and C. Dimitropoulos, Phys. Rev. Lett. **96**, 097201 (2006).
[44]V. Kiryukhin, Y. J. Wang, F. C. Chou, M. A. Kastner, and R. J. Birgeneau, Phys. Rev. B **59**, R6581 (1999).
[45]D. Casa, B Keimer, M. V. Zimmermann, J. P. Hill, H. U. Habermeier, and F. S. Razavi, Phys. Rev. B **64**, 100404 (2001).
[46]M. Hervieu, A. Barnabé, C. Martin, A. Maignan, and B. Raveau, Phys. Rev. B **60**, R726 (1999).
[47]Y. Horibe, C. H. Chen, S.-W. Cheong, and S. Mori, Europhys. Lett. **70**, 383 (2005).